Probing robust Majorana signatures by crossed Andreev reflection with a quantum dot

Guan-Hao Feng and Hong-Hao Zhang [*]

Guangdong Key Laboratory of Magnetoelectric Physics and Devices, School of Physics, Sun Yat-sen University, Guangzhou 510275, China

We propose a three-terminal structure to probe robust signatures of Majorana zero modes. This structure consists of a quantum dot coupled to the normal-metal, s-wave superconducting, and Majorana Y-junction leads. The zero-bias differential conductance at zero temperature of the normal-metal lead peaks at $2e^2/h$, which will be deflected after Majorana braiding. This quantized conductance can entirely arise from the Majorana-induced crossed Andreev reflection, protected by the energy gap of the superconducting lead. We find that the effect of thermal broadening is significantly suppressed when the dot is on resonance. In the case in which the energy level of the quantum dot is much larger than the superconducting gap, tunneling processes are dominated by Majorana-induced crossed Andreev reflection. Particularly, a novel kind of crossed Andreev reflection equivalent to the splitting of charge quanta $3e$ occurs after Majorana braiding.

I. INTRODUCTION

Majorana zero modes (MZMs) are zero-energy quasiparticle excitations originating from coherent superpositions of electrons and holes. Following theoretical suggestions, MZMs are supported in 1D systems, such as InAs or InSb wires with strong spin-orbit coupling and proximity-induced superconductivity [1,2], and they show great potential in decoherence-free quantum computation [3–6]. Verifying the existence of MZMs and their non-Abelian braiding has been attracting much attention in recent years [7–16].

Due to the property that an MZM can act as both an electron lead and a hole lead in tunneling processes, one of the most exciting theoretical predictions is a quantized zero-bias conductance peak (ZBCP) of $\frac{2e^2}{h}$ at zero temperature [17–19]. However, it is quite difficult to observe this quantization from a direct junction between a normal-metal lead and MZMs in a single-subband wire because of thermal broadening, overlap of Majorana wave functions, disorder, and localized Andreev bound states [8,20–25]. Although the observation of ZBCPs has been reported in many experiments in recent years [26–30], the observation of MZMs has not been fully confirmed. Importantly, very recently it has been recognized that one needs to be cautious about the interpretation of nonquantized ZBCPs as the signature of MZMs in local tunneling experiments since such experiments only measure one end of the one-dimensional setup [31], while the most important characteristics of MZMs are their nonlocal correlations. To advance the pursuit of MZMs, new theoretical proposals and new signatures which can reflect the nonlocal correlations of MZMs are hence highly demanded. For example, shot noise and the Fano factor in Majorana setups can carry interesting information to identify MZMs [7,15,16,32–38].

Here we propose a T-shaped hybrid structure to detect MZMs, as illustrated in Fig. 1. The central quantum dot (QD) acts as a transfer station of electrons and holes. Hence tuning the energy level of the QD is equivalent to tuning the transmission coefficients. The key to probe MZMs is the Majorana-induced crossed Andreev reflection [18,32,39,40]. The ZBCP arising from the crossed Andreev reflection in this T-shaped structure is strongly protected by the energy gap of the superconducting lead because quasiparticle excitations are exponentially suppressed $\sim \exp(-\Delta/T)$. Such kinds of multiterminal structures with a QD show excellent maneuverability in the studies of spin-dependent transport in strong Coulomb-correlated systems [41–47].

At zero temperature, we find that the ZBCP of the normal-metal lead is quantized to $2e^2/h$ before braiding, which can be completely induced by the crossed Andreev reflection. This quantized ZBCP is found to be considerably robust against the temperature when the QD is on resonance ($\epsilon_d = 0$). We show that the crossed Andreev reflection dominates over the conventional Andreev reflection when $\epsilon_d \gg \Delta$. Importantly, we find that the Majorana braiding shifts the ZBCPs and arouses a novel kind of crossed Andreev reflection equivalent to the splitting of $3e$ charge quanta, as shown in Fig. 5. Because of the high controllability of QD and the robustness of the predicted signatures, our findings suggest a promising new way to identify MZMs.

It is worth noting that while the Kondo correlations are important in a strong-coupling and low-temperature regime, the Kondo resonances are usually either unstable or unquantized [48–50]. In sharp contrast, the Majorana-induced resonance in this paper is always singly situated at zero bias and leads to quantized conductance. In order to isolate and investigate observable consequences of the Majorana-induced subgap resonances, we neglect the Kondo correlations and focus on the Majorana-induced crossed Andreev reflection.

This paper is organized as follows. In Sec. II, we introduce the T-shaped hybrid model and explicitly write down its

---

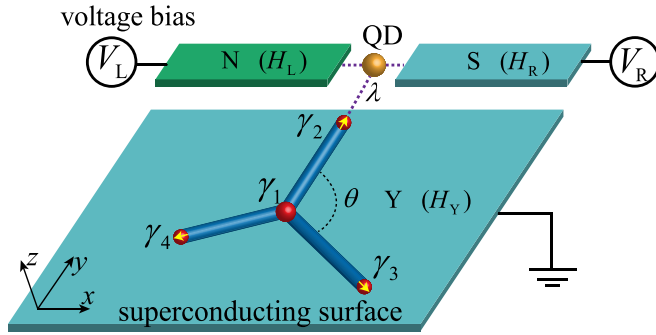*Corresponding author: zhh98@mail.sysu.edu.cn

FIG. 1. Setup of the T-shaped QD-(N, S, Y) model with the normal-metal lead (N), the superconducting lead (S), and the Majorana Y-junction lead (Y). Following Refs. [51,52], the Majorana braiding can be implemented on the Y junction by tuning the couplings between the MZMs.

Hamiltonians. In Sec. III, we discuss the electronic transport of the system and provide the corresponding current and conductance formulas, including the analytical expressions for the ZBCPs. In Sec. IV, we present the formula for the shot noise and the Fano factor in terms of appropriate Green's functions. The detailed derivations of the self-energy, the local density of states, and the shot noise are given in Appendices A, B, and C, respectively.

II. MODEL AND FORMULATION

We introduce the three-terminal setup shown in Fig. 1. The three leads are coupled with a central QD and the superconducting lead ensures that the occurrence of crossed Andreev reflection, which protects the ZBCP from quasiparticle excitations. The tunnel-coupled structure can be described by an effective low-energy Hamiltonian:

$$H = H_L + H_R + H_{QD} + H_Y + H_T. \quad (1)$$

The first term in Eq. (1) is the Hamiltonian of the normal-metal lead (N) in Fig. 1, which is characterized by

$$H_L = \sum_{k\sigma} \epsilon_{L,k\sigma} a^\dagger_{L,k\sigma} a_{L,k\sigma}, \quad (2)$$

where $a^\dagger_{L,k\sigma}$ ($a_{L,k\sigma}$) are creation (annihilation) operators with wave vector k and spin $\sigma = \uparrow, \downarrow$, and $\epsilon_{L,k\sigma}$ is the corresponding electron energy. The second term, the Hamiltonian of the superconducting lead (S) in Fig. 1, is given by the BCS theory,

$$H_R = \sum_{k\sigma} \epsilon_{R,k\sigma} a^\dagger_{R,k\sigma} a_{R,k\sigma} + \sum_k (\Delta a^\dagger_{R,k\uparrow} a^\dagger_{R,-k\downarrow} + \text{H.c.}). \quad (3)$$

The superconducting energy gap Δ is real here since a unitary transformation has been performed on this Hamiltonian [45,53]. In this work, we set the applied voltage of the superconducting lead $V_R = 0$. For simplicity, we use the non-interacting Hamiltonian of the QD,

$$H_{QD} = \sum_\sigma \epsilon_d d^\dagger_\sigma d_\sigma, \quad (4)$$

where the QD level $\epsilon_d = \epsilon_0 - eV_g/2$ is controlled by a gate voltage V_g [9,47,48]. The Hamiltonian of the Majorana Y

junction (Y) in Fig. 1 is given by

$$H_Y = i \sum_{k=2}^4 t_{1k} \gamma_1 \gamma_k, \quad (5)$$

where the Coulomb coupling constants are $t_{12} = t_{13} = t_{min}$ and $t_{14} = t_{max}$ with $t_{min} \ll t_{max}$ [51]. Using two fermionic operators $c_1 = (\gamma_1 - i\gamma_4)/2$ and $c_2 = (\gamma_2 - i\gamma_3)/2$, the Hamiltonian H_Y can be represented in the four-dimensional Nambu-spinor space spanned by $c^\dagger_Y = (c^\dagger_1, c_1, c^\dagger_2, c_2)$.

The tunneling Hamiltonian consists of

$$H_T = H_{T,L} + H_{T,R} + H_{T,Y}, \quad (6)$$

where

$$H_{T,L(R)} = \sum_{k\sigma} v_{L(R),k} d^\dagger_\sigma a_{L(R),k\sigma} + \text{H.c.}, \quad (7)$$

with $v_{L,k}$ and $v_{R,k}$ denoting the complex tunneling amplitudes of the normal-metal and superconducting leads, respectively. The coupling between the QD and the Majorana lead is spin conserving; i.e., the MZM is always tunnel-coupled to electrons in the QD with the same spin orientation [54]. Since we have set the spin orientation of the Rashba spin-orbit coupling along the z direction in Fig. 1, the spin of each MZM (except γ_1) is parallel to the axial direction of the corresponding nanowire [2,55]. Defining that the spin-$\uparrow$ direction is along the y direction, the coupling between the QD and the Majorana lead is given by

$$H_{T,Y} = \lambda d^\dagger_\uparrow \gamma_2 + \text{H.c.}, \quad (8)$$

where λ is the coupling amplitude. For simplicity, we assume λ is real.

III. CURRENT AND CONDUCTANCE

The ZBCP arising from the crossed Andreev reflection in this T-shaped structure is a remarkable signature of MZMs. In this section, we first calculate the time-average current by using the nonequilibrium Green's function method [15,53,56–59], and then derive the analytic expression of the ZBCP of each lead.

The time-average current of the normal-metal lead is given by

$$I_L = -e\langle \dot{N}_L(t) \rangle$$
$$= \frac{e}{h} \int d\omega \, \text{Re Tr} \left\{ \left[G^R_{QD}(\omega) \Sigma^<_L(\omega) + G^<_{QD}(\omega) \Sigma^A_L(\omega) \right] \tilde{\sigma}_z \right\}, \quad (9)$$

where $N_L(t) = \sum_{k\sigma} a^\dagger_{L,k\sigma}(t) a_{L,k\sigma}(t)$ is the total number operator of the electrons in the normal-metal lead. The 4×4 Green's functions $G^<_{QD}(t,t') \equiv -i\langle d(t') d^\dagger(t) \rangle$ and $G^R_{QD}(t,t') \equiv -i\theta(t-t') \langle \{d(t), d^\dagger(t')\} \rangle$ are defined with the Nambu spinors $d^\dagger = (d^\dagger_\uparrow, d_\downarrow, d^\dagger_\downarrow, d_\uparrow)$. The retarded self-energy $\Sigma^R_L(\omega) = [\Sigma^A_L(\omega)]^\dagger = \sum_k \mathcal{H}_{T,L} g^R_L(\omega) \mathcal{H}_{T,L}$ is defined with the Nambu spinors $a^\dagger_{L(R)} = (a^\dagger_{L(R),k\uparrow}, a_{L(R),-k\downarrow}, a^\dagger_{L(R),-k\downarrow}, a_{L(R),k\uparrow})$. Here $g^R_L(\omega) = (\omega - \mathcal{H}_L + i0^+)^{-1}$ is the corresponding unperturbed Keldysh contour Green's functions of the normal-metal lead. The lesser self-energy is $\Sigma^<_L(\omega) = F_L(\Sigma^A_L(\omega) - \Sigma^R_L(\omega))$, where $F_L =$

diag$(f_L, \bar{f}_L, f_L \bar{f}_L)$ is the Fermi distribution function matrix with $f_L = f(\omega - eV_L)$ and $\bar{f}_L = f(\omega + eV_L)$. The matrix $\tilde{\sigma}_z = \text{diag}(1, -1, 1, -1)$ describes the different charge of electrons and holes.

The time-average current Eq. (9) is calculated in terms of $\Sigma_L^{R,A,<}(\omega)$ and $G_{QD}^{R,A,<}(\omega)$. This expression can be generalized to I_η by replacing the self-energies $\Sigma_L^{R,A,<}(\omega)$ with $\Sigma_\eta^{R,A,<}(\omega)$ for $\eta = $ L, R, and Y representing the normal-metal lead, the superconducting lead, and the Majorana lead, respectively. In the basis $(d^\dagger, a_L^\dagger, a_R^\dagger, c_Y^\dagger)$, the Hamiltonian Eq. (1) can be written in a block form as

$$\mathcal{H} = \begin{pmatrix} \mathcal{H}_{QD} & \mathcal{H}_{T,L} & \mathcal{H}_{T,R} & \mathcal{H}_{T,Y} \\ \mathcal{H}_{T,L}^\dagger & \mathcal{H}_L & 0 & 0 \\ \mathcal{H}_{T,R}^\dagger & 0 & \mathcal{H}_R & 0 \\ \mathcal{H}_{T,Y}^\dagger & 0 & 0 & \mathcal{H}_Y \end{pmatrix}, \quad (10)$$

where the submatrices are given by

$$\mathcal{H}_L = \begin{pmatrix} \epsilon_{L,k\uparrow} & 0 & 0 & 0 \\ 0 & -\epsilon_{L,k\downarrow} & 0 & 0 \\ 0 & 0 & \epsilon_{L,k\downarrow} & 0 \\ 0 & 0 & 0 & -\epsilon_{L,k\uparrow} \end{pmatrix}, \quad (11a)$$

$$\mathcal{H}_R = \begin{pmatrix} \epsilon_{R,k\uparrow} & \Delta & 0 & 0 \\ \Delta & -\epsilon_{R,k\downarrow} & 0 & 0 \\ 0 & 0 & \epsilon_{R,k\downarrow} & -\Delta \\ 0 & 0 & -\Delta & -\epsilon_{R,k\uparrow} \end{pmatrix}, \quad (11b)$$

$$\mathcal{H}_{QD} = \begin{pmatrix} \epsilon_d & 0 & 0 & 0 \\ 0 & -\epsilon_d & 0 & 0 \\ 0 & 0 & \epsilon_d & 0 \\ 0 & 0 & 0 & -\epsilon_d \end{pmatrix}, \quad (11c)$$

$$\mathcal{H}_Y = \begin{pmatrix} -2t_{14} & 0 & it_{12} - t_{13} & it_{12} + t_{13} \\ 0 & 2t_{14} & it_{12} - t_{13} & it_{12} + t_{13} \\ -it_{12} - t_{13} & -it_{12} - t_{13} & 0 & 0 \\ -it_{12} + t_{13} & -it_{12} + t_{13} & 0 & 0 \end{pmatrix}, \quad (11d)$$

$$\mathcal{H}_{T,L(R)} = \begin{pmatrix} v_{L(R),k} & 0 & 0 & 0 \\ 0 & -v_{L(R),k}^* & 0 & 0 \\ 0 & 0 & v_{L(R),k} & 0 \\ 0 & 0 & 0 & -v_{L(R),k}^* \end{pmatrix}, \quad (11e)$$

$$\mathcal{H}_{T,Y} = \begin{pmatrix} 0 & 0 & \lambda & \lambda \\ 0 & 0 & 0 & 0 \\ 0 & 0 & 0 & 0 \\ 0 & 0 & -\lambda & -\lambda \end{pmatrix}. \quad (11f)$$

Assuming that the electron energies in Eqs. (2) and (3) are independent of spins with $\epsilon_{L(R),k\uparrow} = \epsilon_{L(R),k\downarrow} = \epsilon_{L(R),k}$, the retarded self-energies from the couplings between the three leads and the QD are given by

$$\Sigma_L^R(\omega) = -\frac{i}{2}\Gamma_L \begin{pmatrix} 1 & 0 & 0 & 0 \\ 0 & 1 & 0 & 0 \\ 0 & 0 & 1 & 0 \\ 0 & 0 & 0 & 1 \end{pmatrix}, \quad (12)$$

$$\Sigma_R^R(\omega) = -\frac{i}{2}\Gamma_R\beta(\omega) \begin{pmatrix} 1 & -\frac{\Delta}{\omega} & 0 & 0 \\ -\frac{\Delta}{\omega} & 1 & 0 & 0 \\ 0 & 0 & 1 & \frac{\Delta}{\omega} \\ 0 & 0 & \frac{\Delta}{\omega} & 1 \end{pmatrix}, \quad (13)$$

$$\Sigma_Y^R(\omega) = \kappa\Lambda = \kappa \begin{pmatrix} 1 & 0 & 0 & -1 \\ 0 & 0 & 0 & 0 \\ 0 & 0 & 0 & 0 \\ -1 & 0 & 0 & 1 \end{pmatrix}, \quad (14)$$

where $\Gamma_{L(R)} = 2\pi|v_{L(R),k}|^2 \rho_{L(R)}$ is the linewidth function with $\rho_{L(R)}$ being the density of normal states. In the wide-band limit, $\Gamma_{L(R)}$ is a constant independent of the frequency ω. Here $\beta(\omega) = \frac{|\omega|\Theta(|\omega| - \Delta)}{\sqrt{\omega^2 - \Delta^2}} + \frac{\omega\Theta(\Delta - |\omega|)}{i\sqrt{\Delta^2 - \omega^2}}$ is the dimensionless BCS density of states. Neglecting the contribution of t_{min}, we have $\kappa \approx \frac{-8\lambda^2 t_{max}^2 + 2\lambda^2(\omega^+)^2}{-4t_{max}^2\omega^+ + (\omega^+)^3}$ with $\omega^+ = \omega + i0^+$.

The lesser Green's function of the QD can be obtained via the Keldysh equation $G_{QD}^<(\omega) = G_{QD}^R(\omega)\Sigma_{TOT}^<(\omega)G_{QD}^A(\omega)$, with $\Sigma_{TOT}^< = \sum_\eta \Sigma_\eta^<$. In the calculation of the time-average current, we can take $\Sigma_Y^< = 0$ (see Appendix A for details). In the case of $|eV_L| < |\Delta|$, analytical calculations for the time-average current yield $I_\eta = \frac{e}{2h}\int d\omega(f_L - \bar{f}_L)T_\eta(\omega)$, which means that only Andreev reflection processes contribute to the electronic transport of the system. Since the system is in a stationary regime, the total current is conserved, i.e., $\sum_\eta I_\eta = 0$.

The differential conductances of the leads η at zero temperature are obtained by $G_\eta = dI_\eta/dV_L$. Especially, the ZBCPs at zero temperature are

$$\lim_{eV_L \to 0} G_L(eV_L) = \begin{cases} \frac{2e^2}{h}, & \lambda \neq 0, \\ \frac{e^2}{h}\frac{16\Gamma_L^2\Gamma_R^2}{(\Gamma_L^2 + \Gamma_R^2 + 4\epsilon_d^2)^2}, & \lambda = 0, \end{cases} \quad (15)$$

$$\lim_{eV_L \to 0} G_R(eV_L) = \begin{cases} -\frac{e^2}{h}\frac{4\Gamma_R^2}{\Gamma_L^2 + \Gamma_R^2 + 4\epsilon_d^2}, & \lambda \neq 0, \\ -\frac{e^2}{h}\frac{16\Gamma_L^2\Gamma_R^2}{(\Gamma_L^2 + \Gamma_R^2 + 4\epsilon_d^2)^2}, & \lambda = 0, \end{cases} \quad (16)$$

$$\lim_{eV_L \to 0} G_Y(eV_L) = \begin{cases} -\frac{e^2}{h}\frac{2(\Gamma_L^2 - \Gamma_R^2 + 4\epsilon_d^2)}{\Gamma_L^2 + \Gamma_R^2 + 4\epsilon_d^2}, & \lambda \neq 0, \\ 0, & \lambda = 0. \end{cases} \quad (17)$$

When $\lambda = 0$, the Majorana Y junction is disconnected with the QD, and the remaining part is reduced to an N-QD-S structure. The maximal ZBCP in Eq. (15) is equal to $4e^2/h$ when the QD is symmetrically coupled ($\Gamma_L = \Gamma_R$) and on resonance ($\epsilon_d = 0$), in accord with the previous results of Ref. [43]. When $\lambda \neq 0$, the ZBCP of the normal-metal lead in this three-terminal structure equals a quantized value $2e^2/h$, which is consistent with the famous conductance peak for the normal metal–topological superconductor tunneling. As depicted in Figs. 2(a)–2(c), the ZBCP is obviously broad for $\epsilon_d = 0$ and becomes sharp for large ϵ_d. The QD acts as a transfer station of electrons and holes, which means that the energy level of the QD is the tunnel barrier of the system. Hence the broadening of the ZBCP arises from the junction transparency effect and the height of the ZBCP is not affected. This quantized ZBCP is caused by the perfect Majorana-induced Andreev reflection. In the next section, we will show that the local Andreev reflection can be completely suppressed by increasing ϵ_d, and only the crossed Andreev reflection remains.
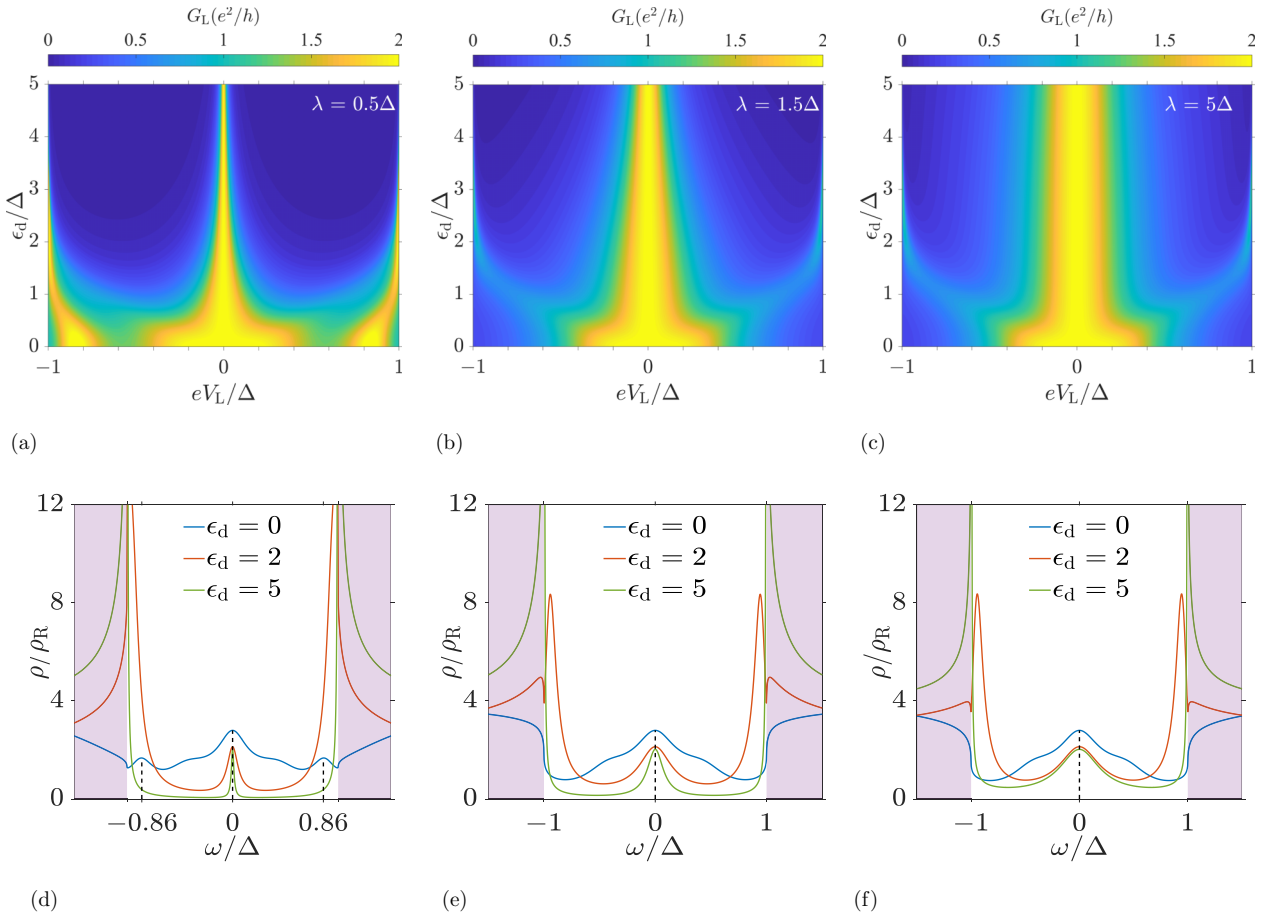
FIG. 2. (a)–(c) Differential conductance spectra of the normal-metal lead as functions of eV_L/Δ and ϵ_d/Δ at zero temperature. The parameters are $\Gamma_L = \Gamma_R = 0.8\Delta$, $t_{min} = 0.001\Delta$, and $t_{max} = \Delta$. (e)–(f) The LDOS of the superconducting lead with the same parameters in (a)–(c). The LDOS is defined by the sum of the diagonal spectral function of the superconducting lead, i.e., $\rho(\omega) = -\text{Im}[\text{Tr } G_R^R]/\pi$.

We emphasize again that this ZBCP of $2e^2/h$ can completely arise from the crossed Andreev reflection, which is strongly protected by the superconducting gap Δ [21]. Moreover, the results of Eqs. (16) and (17) show that the ZBCPs of both the superconducting and the Majorana leads are insensitive to the nonzero coupling amplitude λ, but only dependent on Γ_L, Γ_R, and ϵ_d.

The conductance peaks of the normal-metal lead are closely related to the local density of states (LDOS) of the superconducting lead in this T-shaped structure (the details of the analytical derivation of the LDOS are provided in Appendix B). As shown in Figs. 2(d)–2(f), there are three subgap resonances in the superconducting lead; two are the spin-induced resonances situated near the gap edge [48], and one is the Majorana-induced resonance situated at $\omega = 0$. The conductance peaks are all situated at the subgap resonance energy. As ϵ_d increases, all the resonances become sharper, and the two near the gap edge merge with the dips eventually, whereas the one at $\omega = 0$ remains. For large ϵ_d, the Majorana-induced resonance situated at $\omega = 0$ sharpens to form a localized bound state, i.e., a Yu-Shiba-Rusinov (YSR) state. The occurrence of the Majorana-induced YSR state will lead to the domination of crossed Andreev reflection, which will be discussed in the next section. The Majorana-induced

resonance in the superconducting lead is not quantized but parameter dependent, consistent with the result in Eq. (16). The Majorana-induced resonance leads to a quantized ZBCP of the normal-metal lead since the electrons and holes are transported through perfect Andreev reflection [60]. The spin-induced conductance peaks are unstable and unquantized; i.e., they are not robust as functions of parameters. When λ increases, the Majorana induced resonance is enhanced and the spin-induced conductance peaks become inconspicuous in Figs. 2(b) and 2(c) due to the competition between the spin-induced and the Majorana-induced resonances in the tunneling processes.

The discussion can easily extend to finite-temperature regimes. As shown in Fig. 3, the ZBCP of the normal-metal lead is no longer quantized to $2e^2/h$, since the Fermi distribution is smoothly dependent on the temperature T, which is called the thermal broadening. Nevertheless, we find that the effect of the thermal broadening is significantly suppressed by large junction transparency ($\epsilon_d = 0$). In Fig. 3, the ZBCP is pretty close to $2e^2/h$ when $k_B T < \Delta/20$. Such a temperature condition can be met in experiment; e.g., see Ref. [27], in which the induced superconducting gap of the InSb nanowires is $\Delta \approx 250 \, \mu\text{eV}$ and the minimized temperature is $k_B T \approx 4.3 \, \mu\text{eV}$.
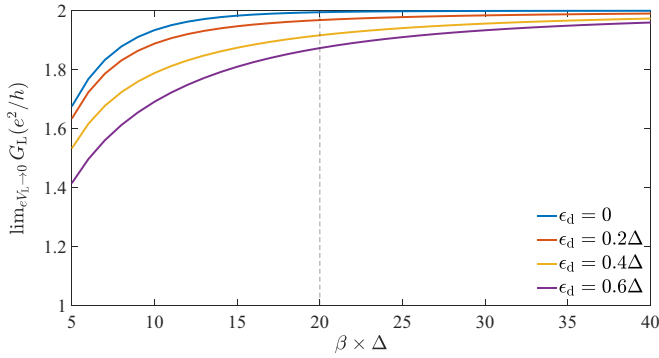
FIG. 3. ZBCP of the normal-metal lead as a function of finite temperature. The parameters are $\Gamma_L = \Gamma_R = 0.8\Delta$, $\lambda = \Delta$, $t_{min} = 10^{-3}\Delta$, and $t_{max} = \Delta$.

IV. SHOT NOISE AND FANO FACTOR

In addition to the time-average current, the shot noise can reveal the fluctuation of the current and provide useful information about MZMs [7,32,35,61]. The shot noise, defined as the correlation function of the current fluctuations between leads η and η', takes the form $S_{\eta\eta'}(t, t') = \langle\{\delta I_\eta(t), \delta I_{\eta'}(t')\}\rangle$, where $\delta I_\eta(t) = \hat{I}_\eta(t) - I_\eta$, and $\hat{I}_\eta(t) = -e\dot{N}_\eta(t)$. The time-average current I_η has been obtained by Eq. (9). With the use of the Wick's theorem and the S-matrix expansion [15,47], we can reduce the expression of the shot noise in terms of Green's functions. After Fourier transform, we obtain the expression of shot noise in the frequency space $S_{\eta\eta'}(\omega')$. The calculation of the shot noise is shown explicitly in Appendix C.

Following Ref. [62], in multiterminal systems, the shot noise $S_{\eta\eta'}(\omega')$ with $\eta = \eta'$ must be positive; conversely, that with $\eta \neq \eta'$ must be negative. This property can be verified by the numerical calculation of $S_{\eta\eta}(0)$ in the following. The zero-frequency Fano factor, defined by the ratio $F_\eta = S_{\eta\eta}(0)/2eI_\eta$, can gain insight into the nature of charge quanta transferred to lead η [35,63,64]. Beyond the linear regime in this paper, the Majorana-induced nonlinear effective charge has been studied in detail [38], which gives rise to fractional effective charge quanta.

The discussion will focus on the case of small transparency ($\epsilon_d \gg \Delta$) since we find that the Fano factors are quantized in this regime. In Fig. 4, we present the Fano factors at zero temperature as functions of ϵ_d/Δ for a specific realization. In the case of $\lambda = 0$, the remaining N-QD-S junction shows a doubled shot noise in Fano factors $F_L(\epsilon_d \gg \Delta) = -F_R(\epsilon_d \gg \Delta) = 2$ due to the transport of Cooper pairs through conventional Andreev reflection [65]. When the Majorana Y junction is connected to the QD with $\lambda \neq 0$, we find $F_L(\epsilon_d \gg \Delta) = -F_Y(\epsilon_d \gg \Delta) = 1$ and $|F_R(\epsilon_d \gg \Delta)| = 2$. The results denote that the unit of charge transferred between the QD and the normal-metal lead is e as well as the Majorana lead, while the unit of charge transferred between the QD and the superconducting lead is $2e$. This is the process of the first kind of crossed Andreev reflection. A hole from the left lead is reflected as an electron into the Majorana lead, while a Cooper pair from the superconducting lead is reflected as a hole into the Majorana lead and an electron into the normal-metal lead [32], as shown in Fig. 5. The holes transferred through crossed
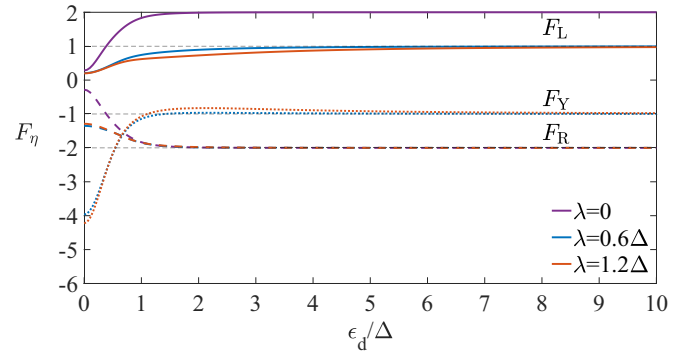

FIG. 4. Fano factors at zero temperature of the left lead (solid lines), right lead (dashed lines), and Majorana lead (dotted lines) as functions of ϵ_d. The parameters are $eV_L = 0.5\Delta$, $\Gamma_L = \Gamma_R = 0.8\Delta$, $t_{min} = 0.001\Delta$, and $t_{max} = \Delta$.

Andreev reflection act as facilitators to propel the splitting of Cooper pairs, and do not contribute to the transferred charge. In this regime, local Andreev reflection is fully suppressed, and the first kind of crossed Andreev reflection dominates.

The quantized Fano factors result from the occurrence of the YSR state below the gap. As shown in Fig. 2(d), a very sharp Majorana-induced midgap resonance at $\omega = 0$ when $\epsilon_d \gg \Delta$ is regarded as a YSR bound state. The occurrence of the YSR state means that the Cooper pairing is "softened" so that the free electrons from the superconducting lead screen the spins of the QD [66,67]. The state-screened process leads to the splitting of Cooper pairs. In this way, crossed Andreev reflection dominates the tunneling processes, which gives rise to the quantized Fano factor.

V. SIGNATURES OF THE MAJORANA BRAIDING

Now we braid the MZMs by taking $\gamma_2 \rightarrow -\gamma_3$ and $\gamma_3 \rightarrow \gamma_2$. Since the spin orientations of the MZMs γ_2 and γ_3
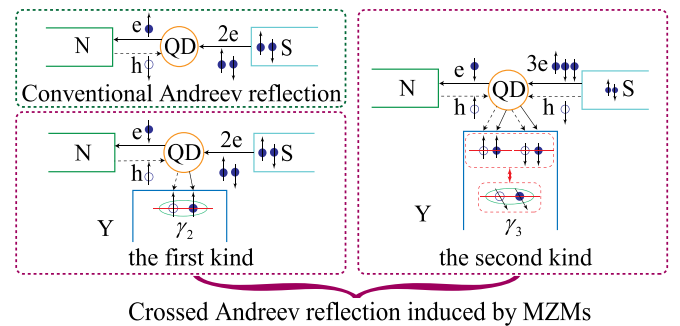

Crossed Andreev reflection induced by MZMs

FIG. 5. When the Majorana lead is disconnected to the QD ($\lambda = 0$), electrons in the S lead are transferred to the N lead through conventional Andreev reflection; when the Majorana lead is connected to the QD ($\lambda \neq 0$), the MZM γ_2 is the coherent superposition of electrons and holes with only spin $\uparrow$, which leads to the first kind of crossed Andreev reflection. After braiding, the MZM γ_3 is coupled to the QD. Since γ_3 is the coherent superposition of electrons and holes with spins $\uparrow$ and $\downarrow$, the second kind of crossed Andreev reflection occurs, which is equivalent to the splitting of charge quanta $3e$. We stress that both kinds of crossed Andreev reflection exist simultaneously after braiding.
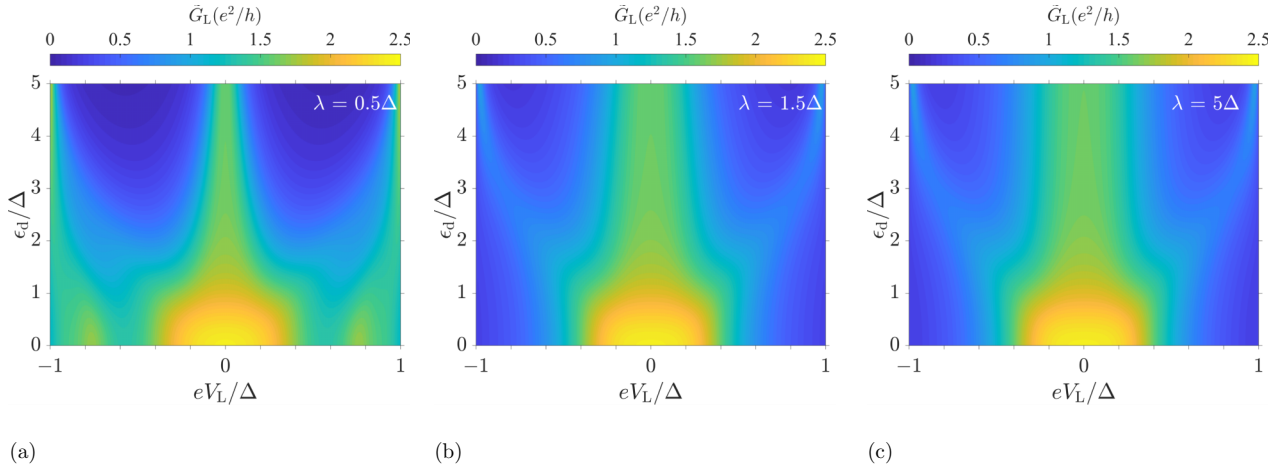
FIG. 6. Differential conductance spectra of the normal-metal lead as a function of $eV_{\rm L}/\Delta$ and $\epsilon_{\rm d}/\Delta$ after braiding at zero temperature. The parameters are the same as in Fig. 2.

belonging to the same complex fermion c_2 are different, observable consequences can be obtained with the connection to the QD. The QD is connected to the Majorana Y junction through γ_3. Using the Nambu spinors and Eq. (5), we can easily obtain the Hamiltonian of the Majorana Y junction $\widetilde{\mathcal{H}}_{\rm Y}$ after braiding. Given that the angle of spin orientations between γ_2 and γ_3 is θ, the spin-conserving coupling is then given by $\widetilde{H}_{\rm T,Y} = -\lambda \widetilde{d}_\uparrow \gamma_3 + {\rm H.c.}$, where $\widetilde{d}_\uparrow$ ($\widetilde{d}_\downarrow$) are the electron operators of the QD with the same (opposite) spin orientation described by γ_3 with

$$\begin{pmatrix} \widetilde{d}_\uparrow \\ \widetilde{d}_\downarrow \end{pmatrix} = \begin{pmatrix} \cos\frac{\theta}{2} & \sin\frac{\theta}{2} \\ -\sin\frac{\theta}{2} & \cos\frac{\theta}{2} \end{pmatrix} \begin{pmatrix} d_\uparrow \\ d_\downarrow \end{pmatrix}. \tag{18}$$

For the Majorana Y junction sketched in Fig. 1, the spin orientation angle is $\theta = \frac{2}{3}\pi$. Such a braiding process is equivalent to involving spin-flip tunneling between the QD and Majorana lead. After braiding, we can obtain the ZBCPs by

$$\lim_{eV_{\rm L}\to 0} \widetilde{G}_{\rm L}(eV_{\rm L}) = \begin{cases} \frac{e^2}{h} \frac{8\Gamma_{\rm L}^2[(\Gamma_{\rm L}^2+\Gamma_{\rm R}^2+4\epsilon_{\rm d}^2)^2+\Gamma_{\rm R}^4+\Gamma_{\rm L}^2\Gamma_{\rm R}^2]}{(4\Gamma_{\rm L}^2+\Gamma_{\rm R}^2)(\Gamma_{\rm L}^2+\Gamma_{\rm R}^2+4\epsilon_{\rm d}^2)^2}, & \lambda \neq 0, \\ \frac{e^2}{h} \frac{16\Gamma_{\rm L}^2\Gamma_{\rm R}^2}{(\Gamma_{\rm L}^2+\Gamma_{\rm R}^2+\epsilon_{\rm d}^2)^2}, & \lambda = 0, \end{cases} \tag{19}$$

$$\lim_{eV_{\rm L}\to 0} \widetilde{G}_{\rm R}(eV_{\rm L}) = \begin{cases} -\frac{e^2}{h} \frac{4\Gamma_{\rm L}^2\Gamma_{\rm R}^2(5\Gamma_{\rm L}^2+5\Gamma_{\rm R}^2+12\epsilon_{\rm d}^2)}{(4\Gamma_{\rm L}^2+\Gamma_{\rm R}^2)(\Gamma_{\rm L}^2+\Gamma_{\rm R}^2+4\epsilon_{\rm d}^2)^2}, & \lambda \neq 0, \\ -\frac{e^2}{h} \frac{16\Gamma_{\rm L}^2\Gamma_{\rm R}^2}{(\Gamma_{\rm L}^2+\Gamma_{\rm R}^2+\epsilon_{\rm d}^2)^2}, & \lambda = 0, \end{cases} \tag{20}$$

$$\lim_{eV_{\rm L}\to 0} \widetilde{G}_{\rm Y}(eV_{\rm L}) = \begin{cases} -\frac{e^2}{h} \frac{4\Gamma_{\rm L}^2(2\Gamma_{\rm L}^2-\Gamma_{\rm R}^2+8\epsilon_{\rm d}^2)}{(4\Gamma_{\rm L}^2+\Gamma_{\rm R}^2)(\Gamma_{\rm L}^2+\Gamma_{\rm R}^2+4\epsilon_{\rm d}^2)}, & \lambda \neq 0, \\ 0, & \lambda = 0. \end{cases} \tag{21}$$

When $\lambda = 0$, the result is the same as that before braiding; when $\lambda \neq 0$, the occurrence of spin-flip tunneling shifts the ZBCP. We plot the differential conductance of the normal-metal lead after the Majorana braiding in Fig. 6 for comparison to Fig. 2. Particularly, if the QD is symmetrically coupled ($\Gamma_{\rm L} = \Gamma_{\rm R} = \Gamma$), the ZBCP of the normal-metal lead maximally shifts to $2.4e^2/h$ for $\epsilon_{\rm d} = 0$ and $1.6e^2/h$ for $\epsilon_{\rm d} \gg \Delta$, which can act a robust hint of Majorana braiding. With the increasing of $\epsilon_{\rm d}$, the ZBCP gets broadened and its

height gets lower concurrently. As shown in Fig. 7, the thermal broadening effect can also be suppressed by taking $\epsilon_{\rm d} = 0$ and each solid line is closed to the corresponding zero-temperature limit when $k_B T < \Delta/20$. Consequently, it is appropriate to observe the ZBCP with large junction transparency.

The Fano factors after braiding are also quantized, but $2 < |\widetilde{F}_{\rm R}(\epsilon_{\rm d} \gg \Delta)| < 3$; i.e., the unit of charge transferred between the QD and the superconducting lead is larger than that of a Cooper pair, as shown Fig. 8. This result is induced by involving both spins $\uparrow$ and $\downarrow$ in the coupling between the QD and the MZM γ_3. As illustrated in Fig. 5, the second kind of crossed Andreev reflection occurs after the Majorana braiding.

Specifically, a Cooper pair transferred between the QD and the superconducting lead is accompanied by an extra electron and a hole, which leads to the $3e$ charge quanta. One electron of the $3e$ charge quanta is reflected as an electron into the normal-metal lead, while the other two are reflected as holes into the Majorana lead. Such a process of charge transmission is equivalent to the splitting of the $3e$ charge quanta.

Given that the electrons coupled to the MZM γ_3 are composed of spin-$\uparrow$ and spin-$\downarrow$ electrons with a certain weight
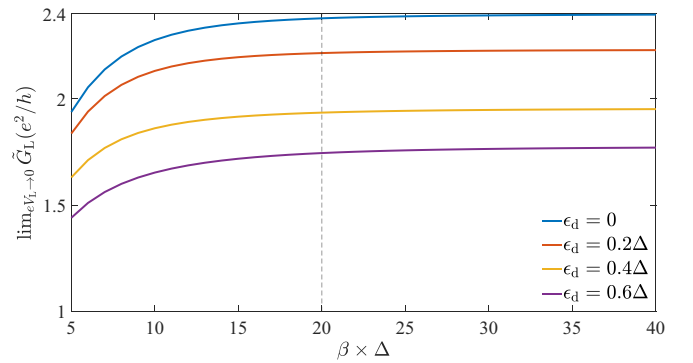

FIG. 7. ZBCP of the normal-metal lead after braiding as a function of the finite temperature. The parameters are the same as in Fig. 3.
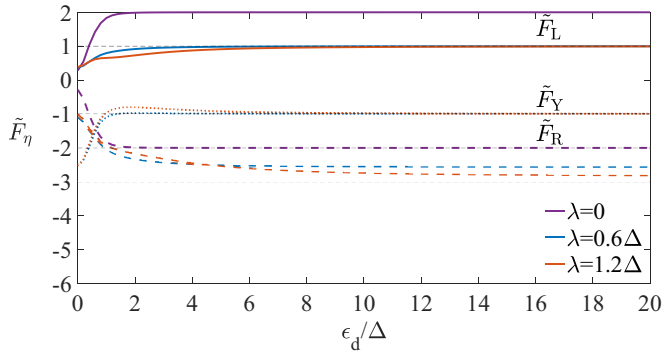
FIG. 8. Fano factors after braiding at zero temperature of the left lead (solid lines), right lead (dashed lines), and Majorana lead (dotted lines) as functions of ϵ_d. The parameters are the same as in Fig. 4.

depending on the angle θ [see Eq. (18)], both kinds of crossed Andreev reflection exist simultaneously, which leads to $2 < |\widetilde{F}_R(\epsilon_d \gg \Delta)| < 3$. As shown in Fig. 8, the second kind of crossed Andreev reflection gains the dominance of the tunneling processes [corresponding to $|\widetilde{F}_R(\epsilon_d \gg \Delta)| \rightarrow 3$] with increasing λ. As for the Majorana lead, the acceptance of spin-$\uparrow$ and spin-$\downarrow$ electrons with a certain weight is equivalent to the acceptance of an electron with spin polarization angle θ in each current pulse, which gives rise to $|\widetilde{F}_Y(\epsilon_d \gg \Delta)| = 1$. The units of the charge transferred between the normal-metal lead and the QD for both kinds of crossed Andreev reflection are identical, so the Fano factor of the normal-metal lead stays at $|\widetilde{F}_L(\epsilon_d \gg \Delta)| = 1$, the same as that before braiding.

VI. CONCLUSION

We have studied the ZBCPs and the Fano factors of the T-shaped structure. We have shown that the ZBCP of the normal-metal lead is always quantized to $2e^2/h$ at zero temperature before braiding, which is quite robust at finite temperature when the QD is on-resonance. This quantized conductance can entirely arise from the Majorana-induced crossed Andreev reflection, which is protected by the energy gap of the superconducting lead. After Majorana braiding, the quantized ZBCP shifts and becomes dependent on the linewidths Γ_L, Γ_R and the QD level ϵ_d. This variation is owing to the introduction of spin-flip tunneling between the Majorana lead and the QD after braiding. By analyzing the quantized Fano factors, we have found that the crossed Andreev reflection dominates over the conventional Andreev reflection when $\epsilon_d \gg \Delta$. We have also found a novel kind of crossed Andreev reflection equivalent to the splitting of the $3e$ charge quanta. The quantized ZBCPs and Fano factors induced by the nonlocal crossed Andreev reflection provide a strong fingerprint for MZMs.

APPENDIX A: CALCULATION OF $\Sigma_Y^<$

In this section, we present the details of the analytical calculation of the terms containing $\Sigma_Y^<$ in Eq. (9). The lesser self-energy from the Majorana lead is given by

$$\Sigma_Y^< = F_Y\left(\Sigma_Y^A - \Sigma_Y^R\right) = -i2F_Y \mathrm{Im}\Sigma_Y^R, \tag{A1}$$

where Σ_Y^R is determined by

$$\kappa \approx \frac{-8\lambda^2 t_{\max}^2}{-4t_{\max}^2\omega^+ + (\omega^+)^3} + \frac{2\lambda^2(\omega^+)^2}{-4t_{\max}^2\omega^+ + (\omega^+)^3}, \tag{A2}$$

with $\omega^+ = \omega + i0^+$, as we mentioned in the main text [κ here is the same as that appearing in Eq. (14)]. We use the notation κ_1 and κ_2 to denote the first term and the second term of κ, respectively. Neglecting the high-order terms of $(i0^+)^{n \geq 2}$, we can obtain the following expressions:

$$\kappa_1 = \frac{-8\lambda^2 t_{\max}^2}{\left(-4t_{\max}^2\omega + \omega^3\right) - \left(4t_{\max}^2 - 3\omega^2\right)(i0^+)}, \tag{A3}$$

$$\kappa_2 = \frac{2\lambda^2\omega^2}{\omega\left(-4t_{\max}^2 + \omega^2\right) + \left(4t_{\max}^2 + \omega^2\right)(i0^+)}. \tag{A4}$$

Using the formula

$$\lim_{\eta \to 0^+} \frac{1}{x \pm i\eta} = \mathcal{P}\frac{1}{x} \mp i\pi\delta(x), \tag{A5}$$

we can obtain

$$i\mathrm{Im}(\kappa_1) = i\pi\frac{-8\lambda^2 t_{\max}^2}{4t_{\max}^2 - 3\omega^2}\delta\left(\frac{-4t_{\max}^2\omega + \omega^3}{4t_{\max}^2 - 3\omega^2}\right), \tag{A6}$$

$$i\mathrm{Im}(\kappa_2) = -i\pi\frac{2\lambda^2\omega^2}{4t_{\max}^2 + \omega^2}\delta\left(\frac{-4t_{\max}^2\omega + \omega^3}{4t_{\max}^2 + \omega^2}\right). \tag{A7}$$

Using the relationship

$$\delta(\phi(x)) = \sum_j \frac{1}{|\phi'(x)|}\delta(x - x_j), \tag{A8}$$

with $\phi(x_j) = 0$, the imaginary parts of κ_1 and κ_2 reduce to

$$i\mathrm{Im}(\kappa_1) = Q_1(\omega)[\delta(\omega) + \delta(\omega - 2t_{\max}) + \delta(\omega + 2t_{\max})], \tag{A9}$$

$$i\mathrm{Im}(\kappa_2) = Q_2(\omega)[\delta(\omega) + \delta(\omega - 2t_{\max}) + \delta(\omega + 2t_{\max})], \tag{A10}$$

where

$$Q_1(\omega) = i\pi \frac{-8\lambda^2 t_{\max}^2}{4t_{\max}^2 - 3\omega^2} \left| \frac{\left(4t_{\max}^2 - 3\omega^2\right)^2}{-\left(4t_{\max}^2 - 3\omega^2\right)^2 - 6\omega^2\left(4t_{\max}^2 - \omega^2\right)} \right|, \tag{A11}$$

$$Q_2(\omega) = -i\pi \frac{2\lambda^2\omega^2}{4t_{\max}^2 + \omega^2} \left| \frac{\left(4t_{\max}^2 + \omega^2\right)^2}{\left(-4t_{\max}^2 + 3\omega^2\right)\left(4t_{\max}^2 + \omega^2\right) - 2\omega^2\left(-4t_{\max}^2 + \omega^2\right)} \right|. \tag{A12}$$

It is obvious that $Q_1(0) = -2i\pi\lambda^2$, $Q_1(\pm 2t_{\max}) = i\pi\lambda^2$, $Q_2(0) = 0$, and $Q_2(\pm 2t_{\max}) = -i\pi\lambda^2$. Since the electron-hole symmetry gives $G_{\mathrm{QD}}^R(-\omega) = -[G_{\mathrm{QD}}^R(\omega)]^*$, i.e., $G_{\mathrm{QD}}^R(0)$ is a purely imaginary function. Note that the imaginary part of $G_{\mathrm{QD}}^R(0)$ is tiny; we can obtain $G_{\mathrm{QD}}^R(0) \approx 0$. For example, the terms containing $\Sigma_{\mathrm{Y}}^<$ in Eq. (9) are calculated by

$$\int d\omega G_{\mathrm{QD}}^R(\omega)\Sigma_{\mathrm{Y}}^<(\omega) \propto \int d\omega G_{\mathrm{QD}}^R(\omega)[i\mathrm{Im}(\kappa_1 + \kappa_2)] = -2i\pi\lambda^2 G_{\mathrm{QD}}^R(0) = 0 \tag{A13}$$

and

$$\int d\omega G_{\mathrm{QD}}^R(\omega)\Sigma_{\mathrm{Y}}^<(\omega)G_{\mathrm{QD}}^A(\omega)\Sigma_{\eta}^A(\omega) = i\pi\lambda^2\left[G_{\mathrm{QD}}^R(0)\Lambda G_{\mathrm{QD}}^A(0)\Sigma_{\eta}^A(0)\right] = 0. \tag{A14}$$

Hence we can take $\Sigma_{\mathrm{Y}}^< = 0$ in the calculation of the time-average current and the shot noise.

APPENDIX B: CALCULATION OF THE LDOS OF THE SUPERCONDUCTING LEAD

For convenience, the whole system is divided into two subsystems, one is "quantum dot + Majorana Y junction + normal-metal lead"; the other is the superconducting lead. The Hamiltonian of the superconducting lead is given by Eq. (3) in the main text,

$$H_{\mathrm{R}} = \sum_{k\sigma} \epsilon_{\mathrm{R},k\sigma} a_{\mathrm{R},k\sigma}^\dagger a_{\mathrm{R},k\sigma} + \sum_k (\Delta a_{\mathrm{R},k\uparrow}^\dagger a_{\mathrm{R},-k\downarrow}^\dagger + \mathrm{H.c.}).$$

In the Nambu space $(a_{\mathrm{R},k\uparrow}^\dagger, a_{\mathrm{R},-k\downarrow}, a_{\mathrm{R},-k\downarrow}^\dagger, a_{\mathrm{R},k\uparrow})$, the unperturbed Green's function of the BCS superconductor evaluated at the origin $(r = 0)$ is represented as

$$g_{\mathrm{R}}^R(\omega) = \int d^3k \frac{e^{ik\cdot r}}{\omega_+^2 - \xi_k^2 - \Delta^2} \begin{pmatrix} \omega_+ + \xi_k & \Delta & & \\ \Delta & \omega_+ - \xi_k & & \\ & & \omega_+ + \xi_k & \Delta \\ & & \Delta & \omega_+ - \xi_k \end{pmatrix}$$

$$= -\rho_R \int d\xi_k \frac{1}{(\xi_k - \sqrt{\omega_+^2 - \Delta^2})(\xi_k + \sqrt{\omega_+^2 - \Delta^2})} \begin{pmatrix} \omega_+ + \xi_k & \Delta & & \\ \Delta & \omega_+ - \xi_k & & \\ & & \omega_+ + \xi_k & -\Delta \\ & & -\Delta & \omega_+ - \xi_k \end{pmatrix},$$

where ρ_R is the density of states and $\omega_+ = \omega + i\eta$ with $\eta = 0^+$. We reduce the expression above by taking

$$\sqrt{\omega_+^2 - \Delta^2} = \sqrt{\omega^2 + i\omega\eta - \Delta^2} \approx \sqrt{\omega^2 - \Delta^2} + i\mathrm{sgn}(\omega)\eta.$$

When $|\Delta| > |\omega|$, the pole (imaginary part > 0) is $\xi_k = i\sqrt{\Delta^2 - \omega^2}$; when $|\Delta| < |\omega|$, the pole (imaginary part > 0) is $\xi_k = i\eta + \mathrm{sgn}(\omega)\sqrt{\omega^2 - \Delta^2}$. Using the theorem of residues, we obtain the unperturbed Green's function of the BCS superconductor as

$$g_{\mathrm{R}}^R(\omega) = \left[-\theta(|\Delta| - |\omega|)\pi\rho_R \frac{1}{\sqrt{\Delta^2 - \omega^2}} - i\theta(|\omega| - |\Delta|)\pi\rho_R \frac{\mathrm{sgn}(\omega)}{\sqrt{\omega^2 - \Delta^2}} \right] \begin{pmatrix} \omega & \Delta & & \\ \Delta & \omega & & \\ & & \omega & -\Delta \\ & & -\Delta & \omega \end{pmatrix}$$

$$= -i\pi\rho_R\beta \begin{pmatrix} 1 & \frac{\Delta}{\omega} & & \\ \frac{\Delta}{\omega} & 1 & & \\ & & 1 & -\frac{\Delta}{\omega} \\ & & -\frac{\Delta}{\omega} & 1 \end{pmatrix},$$

where $\beta(\omega) = \theta(|\Delta| - |\omega|)\frac{\omega}{i\sqrt{\Delta^2 - \omega^2}} + \theta(|\omega| - |\Delta|)\frac{|\omega|}{\sqrt{\omega^2 - \Delta^2}}$.
The spectral function of the superconducting lead is given by

$$A_R(\omega) = i[G_R^R(\omega) - G_R^A(\omega)] = -2\mathrm{Im}G_R^R(\omega)$$

with

$$G_R^R(\omega) = \{[g_R^R(\omega)]^{-1} - \Sigma_{QD}^R(\omega)\}^{-1}.$$

The self-energy at the origin ($r = 0$) can be calculated as

$$
\begin{aligned}
\Sigma_{QD}^R(\omega) &= \sum_k \mathcal{H}_{T,R}^\dagger G_{QD}^R(\omega) \mathcal{H}_{T,R} \\
&= \sum_k |v_{R,k}|^2 G_{QD}^R(\omega) \\
&= 2\pi \rho_R |v_{R,r=0}|^2 G_{QD}^R(\omega) \\
&= \Gamma_R G_{QD}^R(\omega),
\end{aligned}
$$

where we have used Fourier transform $|v_{R,r}|^2 = \frac{1}{2\pi}\sum_k e^{ikr}|v_{R,k}|^2$. The density of states ρ_R around the Fermi surface is approximately regarded as a constant. The effective Green's function of the QD in the subsystem "quantum dot + Majorana Y junction + normal-metal lead" is given by

$$G_{QD}^R(\omega) = \{[g_{QD}^R(\omega)]^{-1} - \Sigma_L^R(\omega) - \Sigma_Y^R(\omega)\}^{-1}.$$

Hence the LDOS of the superconducting lead is

$$\rho(\omega) = \mathrm{Tr}[A_R(\omega)]/2\pi.$$

APPENDIX C: CALCULATION OF THE SHOT NOISE $S_{\eta\eta'}(\omega')$

In this section, we review the formalism for the shot noise which will be used in the main text [15,47]. We consider the Hamiltonian of a multiterminal system with a noninteracting central QD,

$$H = \sum_\eta H_\eta + H_{QD} + H_T, \tag{C1}$$

where $H_\eta = \sum_{k\sigma} \epsilon_{\eta,k\sigma} a_{\eta,k\sigma}^\dagger a_{\eta,k\sigma}$ and $H_{QD} = \sum_\sigma \epsilon_d d_\sigma^\dagger d_\sigma$.

The tunneling Hamiltonian is given by

$$H_T = \sum_{\eta k\sigma}(t_{k\sigma} a_{\eta,k\sigma}^\dagger d_\sigma + t^* d_\sigma^\dagger a_{\eta,k\sigma}), \tag{C2}$$

where $t_{k\sigma}$ is the tunneling amplitude between the leads η and the QD. The definition of the shot noise is given by

$$
\begin{aligned}
S_{\eta\eta'}(t,t') &= \hbar\langle\{\delta\hat{I}_\eta(t), \delta\hat{I}_{\eta'}(t')\}\rangle \\
&= \hbar\langle\{\hat{I}_\eta(t), \hat{I}_{\eta'}(t')\}\rangle - 2\hbar\langle I_\eta(t)\rangle\langle I_{\eta'}(t')\rangle \\
&= -\frac{e^2}{\hbar}\sum_{kk'\sigma\sigma'}\{t_{k\sigma}t_{k'\sigma'}\langle a_{\eta k\sigma}^\dagger(t)d_\sigma(t)a_{\eta'k'\sigma'}^\dagger(t')d_{\sigma'}(t')\rangle \\
&\quad - t_{k\sigma}t_{k'\sigma'}^*\langle a_{\eta k\sigma}^\dagger(t)d_\sigma(t)d_{\sigma'}^\dagger(t')a_{\eta'k'\sigma'}(t')\rangle \\
&\quad - t_{k\sigma}^* t_{k'\sigma'}\langle d_\sigma^\dagger(t)a_{\eta k\sigma}(t)a_{\eta'k'\sigma'}^\dagger(t')d_{\sigma'}(t')\rangle \\
&\quad + t_{k\sigma}^* t_{k'\sigma'}^*\langle d_\sigma^\dagger(t)a_{\eta k\sigma}(t)d_{\sigma'}^\dagger(t')a_{\eta'k'\sigma'}(t')\rangle\} \\
&\quad + \mathrm{H.c.} - 2\hbar\langle I_\eta(t)\rangle\langle I_{\eta'}(t')\rangle. \tag{C3}
\end{aligned}
$$

Using the notation for four types of the two-particle Green's functions,

$$G_1^{(2)}(\tau,\tau') = i^2\langle T_C a_{\eta k\sigma}^\dagger(\tau)d_\sigma(\tau)a_{\eta'k'\sigma'}^\dagger(\tau')d_{\sigma'}(\tau')\rangle, \tag{C4}$$

$$G_2^{(2)}(\tau,\tau') = i^2\langle T_C a_{\eta k\sigma}^\dagger(\tau)d_\sigma(\tau)d_{\sigma'}^\dagger(\tau')a_{\eta'k'\sigma'}(\tau')\rangle, \tag{C5}$$

$$G_3^{(2)}(\tau,\tau') = i^2\langle T_C d_\sigma^\dagger(\tau)a_{\eta k\sigma}(\tau)a_{\eta'k'\sigma'}^\dagger(\tau')d_{\sigma'}(\tau')\rangle, \tag{C6}$$

$$G_4^{(2)}(\tau,\tau') = i^2\langle T_C d_\sigma^\dagger(\tau)a_{\eta k\sigma}(\tau)d_{\sigma'}^\dagger(\tau')a_{\eta'k'\sigma'}(\tau')\rangle, \tag{C7}$$

the shot noise can be expressed as

$$S_{\eta\eta'}(t,t') = \frac{e^2}{\hbar}\sum_{kk',\sigma\sigma'}\{t_{k\sigma}t_{k'\sigma'}G_1^{(2)>}(t,t') - t_{k\sigma}t_{k'\sigma'}^*G_2^{(2)>}(t,t') - t_{k\sigma}^*t_{k'\sigma'}G_3^{(2)>}(t,t') + t_{k\sigma}^*t_{k'\sigma'}^*G_4^{(2)>}(t,t')\} + \mathrm{H.c.} - 2\hbar\langle I_\eta(t)\rangle\langle I_{\eta'}(t')\rangle, \tag{C8}$$

where $G_i^{(2)>}(t,t')$ can be obtained from $G_i^{(2)}(\tau,\tau')$ via analytical continuation. The expression of $G_i^{(2)}(\tau,\tau')$ can be reduced by using the S-matrix expansion and Wick's theorem, and more details can be found in Ref. [47]. After the reduction of $G_i^{(2)}$, we can obtain

$$
\begin{aligned}
G_1^{(2)}(\tau,\tau') = t_{k\sigma}^* t_{k'\sigma'}^* \iint d\tau_1 d\tau_2 G_{\eta,k\sigma\sigma}(\tau_1,\tau)G_{\eta',k'\sigma'\sigma'}(\tau_2,\tau') \\
\times [G_{QD,\sigma\sigma}(\tau,\tau_1)G_{QD,\sigma'\sigma'}(\tau',\tau_2) - G_{QD,\sigma\sigma'}(\tau,\tau_2)G_{QD,\sigma'\sigma}(\tau',\tau_1)], \tag{C9}
\end{aligned}
$$

$$
\begin{aligned}
G_2^{(2)}(\tau,\tau') = -\delta_{kk'\sigma'\sigma'\eta\eta'}G_{\eta,k\sigma'\sigma}(\tau',\tau)G_{QD,\sigma\sigma}(\tau,\tau') + t_{k\sigma}^* t_{k'\sigma'} \iint d\tau_1 d\tau_2 G_{\eta,k\sigma\sigma}(\tau_1,\tau)G_{\eta',k'\sigma'\sigma'}(\tau',\tau_2) \\
\times [G_{QD,\sigma\sigma}(\tau,\tau_1)G_{QD,\sigma'\sigma'}(\tau_2,\tau') - G_{QD,\sigma\sigma'}(\tau,\tau')G_{QD,\sigma'\sigma}(\tau_2,\tau_1)], \tag{C10}
\end{aligned}
$$

$$G_3^{(2)}(\tau,\tau') = [G_2^{(2)}(\tau,\tau')]^*, \tag{C11}$$

$$G_4^{(2)}(\tau,\tau') = [G_1^{(2)}(\tau,\tau')]^*, \tag{C12}$$

where $G_{\eta,k\sigma\sigma}(\tau_1, \tau) = -i\langle T_C a_{\eta k\sigma}(\tau_1) a_{\eta k\sigma}^\dagger(\tau)\rangle$ and $G_{QD,\sigma\sigma'}(\tau, \tau_2) = -i\langle T_C d_\sigma(\tau) d_{\sigma'}^\dagger(\tau_2)\rangle$. The two-particle Green's functions above can be decomposed into the connected and disconnected terms, i.e., $G_i^{(2)}(\tau, \tau') = G_{i,\text{disc}}^{(2)}(\tau, \tau') + G_{i,\text{conn}}^{(2)}(\tau, \tau')$. The disconnected terms are given by

$$G_{1,\text{disc}}^{(2)}(\tau, \tau') = t_{k\sigma}^* t_{k'\sigma'}^* \int d\tau_1 G_{QD,\sigma\sigma}(\tau, \tau_1) G_{\eta,k\sigma\sigma}(\tau_1, \tau^+) \int d\tau_2 G_{QD,\sigma'\sigma'}(\tau', \tau_2) G_{\eta',k'\sigma'}(\tau_2, \tau'^+), \tag{C13}$$

$$G_{2,\text{disc}}^{(2)}(\tau, \tau') = t_{k\sigma}^* t_{k'\sigma'} \int d\tau_1 G_{QD,\sigma\sigma}(\tau, \tau_1) G_{\eta,k\sigma\sigma}(\tau_1, \tau^+) \int d\tau_2 G_{\eta',k'\sigma'\sigma'}(\tau', \tau_2) G_{QD,\sigma'\sigma'}(\tau_2, \tau'^+), \tag{C14}$$

$$G_{3,\text{disc}}^{(2)}(\tau, \tau') = \left[G_{2,\text{disc}}^{(2)}(\tau, \tau')\right]^*, \tag{C15}$$

$$G_{4,\text{disc}}^{(2)}(\tau, \tau') = \left[G_{1,\text{disc}}^{(2)}(\tau, \tau')\right]^*. \tag{C16}$$

The analytic continuation rules give

$$G_{1,\text{disc}}^{(2)>}(t, t') = t_{k\sigma}^* t_{k'\sigma'}^* F_{\eta,k\sigma}(t, t) F_{\eta',k'\sigma'}(t', t'), \tag{C17}$$

$$G_{2,\text{disc}}^{(2)>}(t, t') = -t_{k\sigma}^* t_{k'\sigma'} F_{\eta,k\sigma}(t, t) F_{\eta',k'\sigma'}^*(t', t'), \tag{C18}$$

$$G_{3,\text{disc}}^{(2)>}(t, t') = -t_{k\sigma} t_{k'\sigma'}^* F_{\eta,k\sigma}^*(t, t) F_{\eta',k'\sigma'}(t', t'), \tag{C19}$$

$$G_{4,\text{disc}}^{(2)>}(t, t') = t_{k\sigma} t_{k'\sigma'} F_{\eta,k\sigma}^*(t, t) F_{\eta',k'\sigma'}^*(t', t'), \tag{C20}$$

where

$$F_{\eta,k\sigma}(t, t) = \int dt_1 G_{QD,\sigma\sigma}^R(t, t_1) G_{\eta,k\sigma\sigma}^<(t_1, t) + G_{QD,\sigma\sigma}^<(t, t_1) G_{\eta,k\sigma\sigma}^A(t_1, t). \tag{C21}$$

The total contribution of the disconnected terms is

$$\langle\{\hat{I}_\eta(t), \hat{I}_{\eta'}(t')\}\rangle_{\text{disc}} = \frac{e^2}{\hbar^2} \sum_{kk'\sigma\sigma'} \left\{t_{k\sigma} t_{k'\sigma'} G_{1,\text{disc}}^{(2)>}(t, t') - t_{k\sigma} t_{k'\sigma'}^* G_{2,\text{disc}}^{(2)>}(t, t') - t_{k\sigma}^* t_{k'\sigma'} G_{3,\text{disc}}^{(2)>}(t, t') + t_{k\sigma}^* t_{k'\sigma'}^* G_{4,\text{disc}}^{(2)>}(t, t')\right\} + \text{H.c.}$$

$$= 2\frac{e^2}{\hbar^2} \sum_{kk'\sigma\sigma'} |t_{k\sigma}|^2 |t_{k'\sigma'}|^2 [F_{\eta,k\sigma}(t, t) + F_{\eta,k\sigma}^*(t, t)][F_{\eta',k'\sigma'}(t', t') + F_{\eta',k'\sigma'}^*(t', t')]. \tag{C22}$$

Note that $\Sigma_{\eta,k\sigma\sigma}^< = |t_{k\sigma}|^2 G_{\eta,k\sigma\sigma}^<(t_1, t)$; the time-average current can be written as

$$\langle\hat{I}_\eta(t)\rangle = \frac{e}{\hbar} \sum_{k\sigma} \int dt_1 \left[G_{QD,\sigma\sigma}^R(t, t_1)\Sigma_{\eta,k\sigma\sigma}^< + G_{QD,\sigma\sigma}^<(t, t_1)\Sigma_{\eta,k\sigma\sigma}^A\right] + \text{H.c.},$$

and hence,

$$\langle\hat{I}_\eta(t)\rangle\langle\hat{I}_{\eta'}(t')\rangle = 2\frac{e^2}{\hbar^2} \sum_{kk'\sigma\sigma'} |t_{k\sigma}|^2 |t_{k'\sigma'}|^2 [F_{\eta,k\sigma}(t, t) + F_{\eta,k\sigma}^*(t, t)][F_{\eta',k'\sigma'}(t', t') + F_{\eta',k'\sigma'}^*(t', t')]. \tag{C23}$$

Therefore, the disconnected parts of the shot noise (C22) and (C23) are canceled out:

$$\langle\{\hat{I}_\eta(t), \hat{I}_{\eta'}(t')\}\rangle_{\text{disc}} - 2\langle\hat{I}_\eta(t)\rangle\langle\hat{I}_{\eta'}(t')\rangle = 0. \tag{C24}$$

As a result, the remaining part in the shot noise is only expressed by the connected part by

$$S_{\eta\eta'}(t, t') = \hbar\langle\{\hat{I}_\eta(t), \hat{I}_{\eta'}(t')\}\rangle_{\text{conn}}$$

$$= \frac{e^2}{\hbar} \sum_{kk',\sigma\sigma'} \left\{t_{k\sigma} t_{k'\sigma'} G_{1,\text{conn}}^{(2)>}(t, t') - t_{k\sigma} t_{k'\sigma'}^* G_{2,\text{conn}}^{(2)>}(t, t') - t_{k\sigma}^* t_{k'\sigma'} G_{3,\text{conn}}^{(2)>}(t, t') + t_{k\sigma}^* t_{k'\sigma'}^* G_{4,\text{conn}}^{(2)>}(t, t')\right\} + \text{H.c.}$$

$$= \frac{e^2}{\hbar} \sum_{k,\sigma} |t_{k\sigma}|^2 \delta_{\eta,\eta'} [G_{\eta,k\sigma\sigma}(t', t) G_{QD,\sigma\sigma}(t, t') + G_{\eta,k\sigma\sigma}(t, t') G_{QD,\sigma\sigma}(t', t)]^>$$

$$- \frac{e^2}{\hbar} \sum_{kk',\sigma\sigma'} |t_{k\sigma}|^2 |t_{k'\sigma'}|^2 \left\{\left[\int dt_1 G_{QD,\sigma'\sigma}(t', t_1) G_{\eta,k\sigma\sigma}(t_1, t) \int dt_2 G_{QD,\sigma\sigma'}(t, t_2) G_{\eta',k'\sigma'\sigma'}(t_2, t')\right]^>\right.$$

$$\left. - \left[G_{QD,\sigma'\sigma}(t, t') \iint dt_1 dt_2 G_{\eta,k\sigma\sigma}(t_1, t) G_{QD,\sigma\sigma'}(t_2, t_1) G_{\eta',k'\sigma'\sigma'}(t', t_2)\right]^>\right.$$

$$- \left[G_{\text{QD},\sigma'\sigma}(t',t) \iint dt_1 dt_2 G_{\eta,k\sigma\sigma}(t,t_1) G_{\text{QD},\sigma\sigma'}(t_1,t_2,) G_{\eta',k'\sigma'\sigma'}(t_2,t') \right]^{>}$$

$$+ \left[\int dt_1 G_{\text{QD},\sigma'\sigma}(t_1,t') G_{\eta,k\sigma\sigma}(t,t_1) \int d\tau_2 G_{\text{QD},\sigma\sigma'}(t_2,t) G_{\eta',k'\sigma'\sigma'}(t',t_2) \right]^{>} \Bigg\} + \text{H.c.}$$

$$= \frac{e^2}{\hbar} \text{Tr} \Bigg\{ \delta_{\eta,\eta'} (\Sigma_\eta^{>}(t',t) \widetilde{\sigma}_z G_{\text{QD}}^{<}(t,t') \widetilde{\sigma}_z + G_{\text{QD}}^{>}(t',t) \widetilde{\sigma}_z \Sigma_\eta^{<}(t,t') \widetilde{\sigma}_z)$$

$$- \left[\int dt_1 G_{\text{QD}}(t',t_1) \Sigma_\eta(t_1,t) \right]^{>} \widetilde{\sigma}_z \left[\int dt_2 G_{\text{QD}}(t,t_2) \Sigma_{\eta'}(t_2,t') \right]^{<} \widetilde{\sigma}_z$$

$$+ [G_{\text{QD}}(t,t')]^{>} \widetilde{\sigma}_z \left[\iint dt_1 dt_2 \Sigma_\eta(t_1,t) G_{\text{QD}}(t_2,t_1,) \Sigma_{\eta'}(t',t_2) \right]^{<} \widetilde{\sigma}_z$$

$$+ \left[\iint dt_1 dt_2 \Sigma_\eta(t,t_1) G_{\text{QD}}(t_1,t_2,) \Sigma_{\eta'}(t_2,t') \right]^{>} \widetilde{\sigma}_z [G_{\text{QD}}(t',t)]^{<} \widetilde{\sigma}_z$$

$$- \left[\int dt_1 G_{\text{QD}}(t_1,t') \Sigma_\eta(t,t_1) \right]^{>} \widetilde{\sigma}_z \left[\int dt_2 G_{\text{QD}}(t_2,t) \Sigma_{\eta'}(t',t_2) \right]^{<} \widetilde{\sigma}_z, \tag{C25}$$

where G_{QD} is the 4×4 matrix form of the elements $G_{\text{QD},\sigma'\sigma}$ and Σ_η is the 4×4 matrix form of the elements $\Sigma_{\eta,\sigma\sigma} = \sum_k |t_{k\sigma}|^2 G_{\eta,k\sigma\sigma}$. The matrix $\widetilde{\sigma}_z = \text{diag}(1,-1,1,-1)$ describes the different charge of electrons and holes. Finally, we apply the convolution property of Fourier transform $\int_{-\infty}^{\infty} d(t-t') e^{i\omega'(t-t')} x(t-t') y(t'-t) = \frac{1}{2\pi} \int_{-\infty}^{\infty} d\omega F[x](\omega) F[y](\omega+\omega')$ to the above shot noise and obtain

$$S_{\eta\eta'}(\omega') = \int_{-\infty}^{\infty} d(t-t') e^{i\omega'(t-t')} S_{\eta\eta'}(t-t') = \frac{e^2}{h} \int_{-\infty}^{\infty} d\omega \text{Tr} \{ \delta_{\eta,\eta'} (\Sigma_\eta^{>}(\omega) \widetilde{\sigma}_z G_{\text{QD}}^{<}(\omega+\omega') \widetilde{\sigma}_z + G_{\text{QD}}^{>}(\omega) \widetilde{\sigma}_z \Sigma_\eta^{<}(\omega+\omega') \widetilde{\sigma}_z)$$

$$- [G_{\text{QD}}(\omega) \Sigma_{\eta'}(\omega)]^{>} \widetilde{\sigma}_z [G_{\text{QD}}(\omega+\omega') \Sigma_\eta(\omega+\omega')]^{<} \widetilde{\sigma}_z - [\Sigma_\eta(\omega) G_{\text{QD}}(\omega)]^{>} \widetilde{\sigma}_z [\Sigma_{\eta'}(\omega+\omega') G_{\text{QD}}(\omega+\omega')]^{<} \widetilde{\sigma}_z$$

$$+ G_{\text{QD}}^{>}(\omega) \widetilde{\sigma}_z [\Sigma_{\eta'}(\omega+\omega') G_{\text{QD}}(\omega+\omega') \Sigma_\eta(\omega+\omega')]^{<} \widetilde{\sigma}_z + [\Sigma_\eta(\omega) G_{\text{QD}}(\omega) \Sigma_{\eta'}(\omega)]^{>} \widetilde{\sigma}_z G_{\text{QD}}^{<}(\omega+\omega') \widetilde{\sigma}_z \}. \tag{C26}$$

[1] R. M. Lutchyn, J. D. Sau, and S. Das Sarma, Phys. Rev. Lett. **105**, 077001 (2010).

[2] Y. Oreg, G. Refael, and F. von Oppen, Phys. Rev. Lett. **105**, 177002 (2010).

[3] S. D. Sarma, M. Freedman, and C. Nayak, npj Quantum Inf. **1**, 15001 (2015).

[4] L. Fu and C. L. Kane, Phys. Rev. Lett. **100**, 096407 (2008).

[5] A. C. Potter and P. A. Lee, Phys. Rev. Lett. **105**, 227003 (2010).

[6] A. Y. Kitaev, Phys. Usp. **44**, 131 (2001).

[7] C. J. Bolech and E. Demler, Phys. Rev. Lett. **98**, 237002 (2007).

[8] F. Pientka, G. Kells, A. Romito, P. W. Brouwer, and F. von Oppen, Phys. Rev. Lett. **109**, 227006 (2012).

[9] D. E. Liu and H. U. Baranger, Phys. Rev. B **84**, 201308(R) (2011).

[10] A. R. Akhmerov, J. Nilsson, and C. W. J. Beenakker, Phys. Rev. Lett. **102**, 216404 (2009).

[11] L. Fu and C. L. Kane, Phys. Rev. Lett. **102**, 216403 (2009).

[12] J. Danon, A. B. Hellenes, E. B. Hansen, L. Casparis, A. P. Higginbotham, and K. Flensberg, Phys. Rev. Lett. **124**, 036801 (2020).

[13] A. Haim, E. Berg, F. von Oppen, and Y. Oreg, Phys. Rev. Lett. **114**, 166406 (2015).

[14] L. Fidkowski, J. Alicea, N. H. Lindner, R. M. Lutchyn, and M. P. A. Fisher, Phys. Rev. B **85**, 245121 (2012).

[15] B. H. Wu and J. C. Cao, Phys. Rev. B **85**, 085415 (2012).

[16] T. Jonckheere, J. Rech, A. Zazunov, R. Egger, A. L. Yeyati, and T. Martin, Phys. Rev. Lett. **122**, 097003 (2019).

[17] K. Flensberg, Phys. Rev. B **82**, 180516(R) (2010).

[18] K. T. Law, P. A. Lee, and T. K. Ng, Phys. Rev. Lett. **103**, 237001 (2009).

[19] J. J. He, T. K. Ng, P. A. Lee, and K. T. Law, Phys. Rev. Lett. **112**, 037001 (2014).

[20] D. Bagrets and A. Altland, Phys. Rev. Lett. **109**, 227005 (2012).

[21] Y. Peng, F. Pientka, Y. Vinkler-Aviv, L. I. Glazman, and F. von Oppen, Phys. Rev. Lett. **115**, 266804 (2015).

[22] J. Liu, A. C. Potter, K. T. Law, and P. A. Lee, Phys. Rev. Lett. **109**, 267002 (2012).

[23] O. A. Awoga, J. Cayao, and A. M. Black-Schaffer, Phys. Rev. Lett. **123**, 117001 (2019).

[24] G. Sharma and S. Tewari, Phys. Rev. B **93**, 195161 (2016).

[25] J. Cayao, E. Prada, P. San-Jose, and R. Aguado, Phys. Rev. B **91**, 024514 (2015).

[26] S. Nadj-Perge, I. K. Drozdov, J. Li, H. Chen, S. Jeon, J. Seo, A. H. MacDonald, B. A. Bernevig, and A. Yazdani, Science **346**, 602 (2014).

[27] V. Mourik, K. Zuo, S. M. Frolov, S. Plissard, E. P. Bakkers, and L. P. Kouwenhoven, Science **336**, 1003 (2012).

[28] A. Das, Y. Ronen, Y. Most, Y. Oreg, M. Heiblum, and H. Shtrikman, Nat. Phys. **8**, 887 (2012).

[29] S. Zhu, L. Kong, L. Cao, H. Chen, M. Papaj, S. Du, Y. Xing, W. Liu, D. Wang, C. Shen, F. Yang, J. Schneeloch, R. Zhong, G. Gu, L. Fu, Y.-Y. Zhang, H. Ding, and H.-J. Gao, Science **367**, 189 (2020).

[30] H.-H. Sun, K.-W. Zhang, L.-H. Hu, C. Li, G.-Y. Wang, H.-Y. Ma, Z.-A. Xu, C.-L. Gao, D.-D. Guan, Y.-Y. Li, C. Liu, D. Qian, Y. Zhou, L. Fu, S.-C. Li, F.-C. Zhang, and J.-F. Jia, Phys. Rev. Lett. **116**, 257003 (2016).

[31] S. Frolov, Nature (London) **592**, 350 (2021).

[32] J. Nilsson, A. R. Akhmerov, and C. W. J. Beenakker, Phys. Rev. Lett. **101**, 120403 (2008).

[33] K. M. Tripathi, S. Das, and S. Rao, Phys. Rev. Lett. **116**, 166401 (2016).

[34] D. E. Liu, M. Cheng, and R. M. Lutchyn, Phys. Rev. B **91**, 081405(R) (2015).

[35] A. Golub and B. Horovitz, Phys. Rev. B **83**, 153415 (2011).

[36] D. Giuliano, S. Paganelli, and L. Lepori, Phys. Rev. B **97**, 155113 (2018).

[37] S. Smirnov, Phys. Rev. B **99**, 165427 (2019).

[38] S. Smirnov, New J. Phys. **19**, 063020 (2017).

[39] D. Beckmann, H. B. Weber, and H. v. Löhneysen, Phys. Rev. Lett. **93**, 197003 (2004).

[40] S.-B. Zhang and B. Trauzettel, Phys. Rev. Lett. **122**, 257701 (2019).

[41] A. Cottet, W. Belzig, and C. Bruder, Phys. Rev. Lett. **92**, 206801 (2004).

[42] Y. Zhu, W. Li, T.-h. Lin, and Q.-f. Sun, Phys. Rev. B **66**, 134507 (2002).

[43] X. F. Cao, Y. Shi, X. Song, S. Zhou, and H. Chen, Phys. Rev. B **70**, 235341 (2004).

[44] Y. Zhu, Q.-f. Sun, and T.-h. Lin, Phys. Rev. B **65**, 024516 (2001).

[45] Q.-f. Sun, J. Wang, and T.-h. Lin, Phys. Rev. B **59**, 3831 (1999).

[46] Q.-f. Sun, J. Wang, and T.-h. Lin, Phys. Rev. B **62**, 648 (2000).

[47] F. M. Souza, A. P. Jauho, and J. C. Egues, Phys. Rev. B **78**, 155303 (2008).

[48] V. Koerting, B. M. Andersen, K. Flensberg, and J. Paaske, Phys. Rev. B **82**, 245108 (2010).

[49] M. Cheng, M. Becker, B. Bauer, and R. M. Lutchyn, Phys. Rev. X **4**, 031051 (2014).

[50] G. Kiršanskas, M. Goldstein, K. Flensberg, L. I. Glazman, and J. Paaske, Phys. Rev. B **92**, 235422 (2015).

[51] B. van Heck, A. Akhmerov, F. Hassler, M. Burrello, and C. Beenakker, New J. Phys. **14**, 035019 (2012).

[52] T. Karzig, Y. Oreg, G. Refael, and M. H. Freedman, Phys. Rev. X **6**, 031019 (2016).

[53] J. C. Cuevas, A. Martín-Rodero, and A. Levy Yeyati, Phys. Rev. B **54**, 7366 (1996).

[54] A. Zazunov, R. Egger, and A. Levy Yeyati, Phys. Rev. B **94**, 014502 (2016).

[55] L. Xu, X.-Q. Li, and Q.-F. Sun, J. Phys.: Condens. Matter **29**, 195301 (2017).

[56] Y. Meir and N. S. Wingreen, Phys. Rev. Lett. **68**, 2512 (1992).

[57] H. Haug, A.-P. Jauho *et al.*, *Quantum Kinetics in Transport and Optics of Semiconductors* (Springer, Berlin, 2008), Vol. 2, Chaps. 4 and 12.

[58] Z. Y. Zeng, B. Li, and F. Claro, Phys. Rev. B **68**, 115319 (2003).

[59] L. V. Keldysh *et al.*, Sov. Phys. JETP **20**, 1018 (1965).

[60] H. Pan, C.-X. Liu, M. Wimmer, and S. Das Sarma, Phys. Rev. B **103**, 214502 (2021).

[61] L. Fu and C. L. Kane, Phys. Rev. B **79**, 161408(R) (2009).

[62] Y. Blanter and M. Büttiker, Phys. Rep. **336**, 1 (2000).

[63] R. Cron, M. F. Goffman, D. Esteve, and C. Urbina, Phys. Rev. Lett. **86**, 4104 (2001).

[64] J. C. Cuevas, A. Martín-Rodero, and A. Levy Yeyati, Phys. Rev. Lett. **82**, 4086 (1999).

[65] M. J. M. de Jong and C. W. J. Beenakker, Phys. Rev. B **49**, 16070 (1994).

[66] B. W. Heinrich, J. I. Pascual, and K. J. Franke, Prog. Surf. Sci. **93**, 1 (2018).

[67] R. Maurand and C. Schönenberger, Physics **6**, 75 (2013).